Investigating the Effects of Calcination Temperature on Porous Clay Heterostructure Characteristics

Muhammad Kashif[1,2], Chaeyeon Kang[1], Tatwadhika Rangin Siddhartha[1,2], Clovis Awah Che[1], Yaxin Su[3], Philippe M. Heynderickx[1,2,*]

[1]*Centre for Green Chemistry and Environmental Biotechnology (GREAT) – Engineering of Materials via Catalysis and Characterization, Ghent University Global Campus, 119-5 Songdomunhwa-Ro, Yeonsu-Gu, Incheon, 406-840 South Korea*

[2]*Department of Green Chemistry and Technology, Faculty of Bioscience Engineering, Ghent University, 653 Coupure Links, Ghent, B-9000, Belgium*

[3]*College of Environmental Science and Engineering, Donghua University, Shanghai, 201620, China*

***Corresponding author**

Philippe.Heynderickx@Ghent.ac.kr (Philippe M. Heynderickx)

This study focuses on finding the optimal calcination temperature for synthesizing porous clay heterostructures (PCH). PCH was prepared using montmorillonite at different temperatures (200 to 800°C) in a closed N_2 environment. Samples were characterized via N_2-physisorption, scanning electron microscope (SEM), Fourier-transform infrared spectroscopy (FTIR), X-ray diffraction (XRD), and thermogravimetric analysis (TGA) to investigate the influence of calcination temperature. Characterizations show that the PCH composite exhibits an increasing surface profile observed by increasing specific surface area, changes in crystalline phases, porous surface, and varied particle size distribution. The position (degree and wavelength) and intensities of minerals and functional groups in PCH shift with temperature, as observed in both FTIR and XRD. This shows that variables such as heating rate, calcination temperature, and environment affect the structural changes in the clay material. In terms of active phase development, structural behavior, and material strength, the correct calcination temperature proved to be crucial.

Keywords: Porous clay heterostructures, Montmorillonite, Calcination, N_2-physisorption

Catalysts and their materials are the most important and challenging issues in the industry today. In recent decades, clay minerals have been widely studied and used as catalyst supports in industry and academia for advanced applications, such as isomerization, adsorption (carbon dioxide (CO_2) capture, heavy metals, phenol), photocatalytic reactions, ethanol, hydrogen sulfide (H_2S), and carbon monoxide (CO) oxidation [1,2]. Moreover, owing to their unique properties, such as plasticity, swelling capacity, sorption characteristics, acidic character, ion exchange quality, high-temperature stability and structural properties make clays attractive for various applications, e.g. adsorption and catalysis, and are widely used material in various industries, such as oil and gas, chemical, pharmaceutical, refractory, and ceramics [3,4]. Clay and clay-based catalysts have attracted increasing attention owing to their abundance and low cost. Clays are considered environmentally friendly catalysts as they

are abundant in nature and can be used after minor processing. On the other hand, clay-based catalysts are non-corrosive solids that can be formed into the required shape and size for use in the reactor tube, can be easily separated from the product stream and can be easily disposed of after use without harming the environment.

Porous clay heterostructures (PCH) are newly modified clays with mesoporous and microporous structures. The primary host material for the PCH synthesis is montmorillonite (Mt) lamellar aluminosilicate clay, which has a high cation-exchange nature. The organosilicon source and the cationic surfactant are introduced between clay layers through ion exchange. Finally, by removing the templating agent at the correct calcination temperature, ordered porous materials with micro- and meso-porous structures are produced. The SiO_2 pore walls are solid and stable and have the advantages of hydrophobicity and high thermal stability. They have high research value and high potential for various applications, e.g., nitrogen oxide (NO_x) reduction [1,2], CO_2 capture [3], dyes and heavy metal removal [4–6], water defluoridation [7], pesticides, antibiotics, and phenol adsorption [8,9].

According to previous studies, the ideal calcination temperature for clay-based catalysts generally ranges from 100 to 800°C [10,11]. This temperature range is crucial as it directly affects the physical and chemical characteristics of the materials, such as phase compositions, crystallinity, BET-surface area, and porosity, which are vital for applications in adsorption and catalysis. For example, Wibowo et al. [12] examined the effects of different calcination temperatures on the biodiesel-making ability of lithium-intercalated montmorillonite (Li-K10). The results indicated that 450°C was the optimal calcination temperature for the maximal conversion of methyl laurate. Calcination temperatures below 350°C and above 650°C led to decreased catalytic activity of the Li-K10 catalyst, mostly due to alterations in basicity and structural modifications. A similar behavior was observed in the alumina-based catalyst [13], the Sn-Nb_2O_5/α-Al_2O_3 catalyst employed for ethylene oxide hydration demonstrated an ideal calcination temperature range of 350-400°C. Higher

temperatures result in decreased catalytic efficiency. In general, achieving good catalytic activity or a relation between structure and catalytic performance in clay-based catalysts requires a calcination temperature within the range of 400-800°C. However, the specific ideal temperature may vary depending on the kind of clay and the intended application.

Considering the potential application (NO_x reduction, CO_2 capture, organic reactions and dye removal) of PCH material, it is important to investigate the effects of calcination temperature on the basic properties, such as Brunauer–Emmett–Teller (BET) surface area, pore diameter, crystal size and structural behavior. In this work, a series of PCH samples were obtained at different calcination temperatures (200, 400, 600, and 800°C) under a closed nitrogen (N_2) atmosphere to analyze the effects of the calcination temperature on physicochemical properties. An interesting aspect of our research is the deliberate and systematic variation of temperatures. In contrast to other studies on the PCH which use a fixed calcination temperature (mostly 550°C [14–19] or a limited temperature range), a wider range of temperatures was investigated in our research. Our research supports in determining the ideal calcination temperature for PCH to achieve specific material characteristics. This allows us to better understand how heat treatment affects the structural and functional properties of newly modified PCH. On the other hand, our technique provides a structured approach to improve the production of PCH for specific applications and serves as a useful reference point for future research in this field.

Montmorillonite K10 ($Al_2H_2O_{12}Si_4$, CAS number: 1318-93-0) and sodium chloride (NaCl, 99%, CAS number: 7647-14-5) were purchased from the Sigma Aldrich. The surfactant hexadecyltrimethylammonium chloride ($C_{19}H_{42}CIN$, 99%, CAS number: 112-02-7) was bought from Thermo Scientific. Dodecylamine ($C_{12}H_{27}N$, 99%, CAS number: 124-22-1) and tetraethyl orthosilicate ($C_8H_{20}O_4Si$, 98.5%, CAS number: 78-10-4) were acquired from Daejung, Korea.

Montmorillonite was used as a host clay mineral in this work for the synthesis of PCH. The synthesis of PCH support involves several steps, which were already reported in the previous study [2,20,21] and **Scheme 1** shows a graphical protocol for the PCH synthesis.

For the preparation of PCH material, 2 g of montmorillonite clay was treated with 5.8 g of NaCl in 100 mL of deionized water. After the solution was stirred for 24 h at room temperature, the modified clay was separated from the aqueous solution via centrifugation, followed by 12 h of drying at 110°C. The modified clay was treated with surfactant hexadecyltrimethylammonium chloride in 100 mL of deionized water. After 24 h of stirring at 60°C, the modified clay was separated from its solution by centrifugation, washed with deionized water a pH value of 7 was reached, and then dried at 30°C for another 24 h. The resulting clay was then added into a solution of dodecylamine and tetraethyl orthosilicate (TEOS) with a ratio of 1:20:150. Finally, after 24 h of stirring at room temperature, the modified clay was separated from the mixture via another round of centrifugation and dried for 12h at 110°C. The obtained clay was calcined at varying temperatures of 200, 400, 600, and 800°C for 6 h. To avoid a rapid heating rate, the corresponding calcination temperatures were reached gradually with a gradual heating time of 5°C/min, respectively. After each step or batch, the obtained sample was thoroughly mixed to homogenize the material before further treatment. The calcination process was carried out under controlled conditions (5°C/min, N_2: 0.4 L/min) in a completely closed tube furnace. The samples were heated to the desired calcination temperature at a uniform rate (5°C/min) to minimize the variations caused by different heating rates. The calcination time was strictly controlled and monitored to ensure uniformity of all samples. The calcination atmosphere (N_2: 0.4 L/min) was maintained to prevent oxidation or reduction processes that could alter the properties of the PCH. Control synthesis was performed at regular intervals to check the consistency of the procedures and to confirm the reliability of the results.

The surface morphology of the catalyst was analyzed using a scanning electron microscope (SEM, FEI, Quanta-250) characterized with an image resolution range of low vacuum mode: ≤10.0 nm (3 kV) to high vacuum mode: ≤3.0 nm (30 kV) and acceleration voltage of 0.2～30Kv. Micromeritics Tristar II was used to investigate the catalyst's specific surface area, pore volume, and pore size distribution by N_2 adsorption-desorption. The specific surface area was determined via the BET equation, while the pore size distribution was determined by the Barrett-Joyner-Halenda (BJH) method. Using the t-plot approach, the total pore volume was derived from the adsorption data at the relative pressure of N_2 P/P0 = 0.99. Phase characterization and crystal structure were examined via the XRD test. An 18 KW X-ray diffract meter (Rigaku) with Cu Kα (λ = 0.15406 nm) was used to record the XRD patterns, and it ran at 40 kV and 30 mA. At a scan rate of 2°/min, the samples were scanned within the 5-30° range. By comparing the recorded patterns with the JCPDS standard card in the Jade 6 software, the phase composition was determined. A Fourier Transform Infrared (FTIR) spectrum was used to examine the surface functional groups of PCH using a Nicolet FTIR spectrometer model VERTEX 70. Thermogravimetry analysis (TGA) tests were carried out on a TGA-801 from LECO Corporation. The temperature was varied from 30 to 900°C by a heating rate of 5°C/min. TGA analysis was carried out on PCH samples in open alumina crucibles under the closed N_2 atmosphere. In short, potential sources of error or bias in the characterization techniques were carefully considered and mitigated through rigorous calibration, standardized procedures, and quality control measures. These efforts were considered to ensure the accuracy and reliability of the data obtained from the characterizations, thereby improving the interpretation and validity of the results of our study.

The influence of the calcination temperature on the surface morphology and chemical composition of the PCH powders was investigated using the SEM technique (see **Fig. 1)**. Among the PCH samples, PCH-200 exhibits loss formation, the lowest pore diameter, and well-connected particles with small crystallite size (31 nm), resulting in better surface

154 morphology than other synthesized samples at high calcination temperatures. When calcined
155 at the lower temperature of 200°C, the surface of the PCH sample exhibited small,
156 aggregated, amorphous platelet-like particles with heterotrimeric structure [22]. In contrast, at
157 higher calcination temperatures of 600 and 800°C, larger aggregates mixed with small
158 particles and curling edges were observed, as shown in **Fig. 1**. This shows that the
159 morphology and size of the PCH crystals strongly depend on the calcination temperature. The
160 XRD and surface morphology show that less agglomeration decreases the crystallite size of
161 the catalyst, as presented in **Table 1**. It was found that the PCH-600 and PCH-800 samples
162 had a higher agglomeration rate, resulting in a decrease in crystallite size [22,23]. All PCH
163 samples exhibited different particle sizes and unevenly distributed voids with corrugated
164 surfaces. The changes in surface morphology correspondingly describe that coarseness and
165 hardness occur as a result of temperature variations in the calcination process, leading to
166 changes in the morphology of the particles and the surface profile of the PCH.

167 **Table 1** and **Fig. 2**ab show the physical properties, pore size distribution and the
168 N_2 adsorption-desorption isotherm of the PCH material. It was found that increasing the
169 calcination temperature increased the BET surface area, pore volume, and crystallite size. As
170 shown in **Table 1**, the PCH-400 sample had the highest BET surface area (667 m^2/g) and
171 average crystallite size (56 nm), while PCH-200 had the lowest BET surface area (227 m^2/g),
172 pore volume (0.38 cm^3/g) and crystallite size (31 nm). It is well known that higher calcination
173 temperatures lead to larger crystallites as imperfections, edges, and defects, are removed
174 during heat treatment, resulting in a well-defined pore diameter and crystalline phase [24].
175 Typically, a large BET surface area can provide numerous active sites for catalytic activity,
176 leading to improved catalytic reactions [25]. This phenomenon occurs because the reactants
177 are more readily available to the active sites on the surface of the material. An increased pore
178 volume can also enhance the diffusion, mass transport, and spread of reactants and products,
179 leading to improved catalytic efficiency [26]. The size of the crystallites of the active phases,

such as alumina and silica, can affect catalytic activity. Reduced crystallite sizes typically result in elevated surface energy and a greater number of active sites, which in turn enhances the catalytic activity of PCH material.

The BET analysis **(Fig. 2**b) shows that all samples prepared displayed Type IV adsorption isotherms, with a characteristic H3 hysteresis loop caused by capillary condensation on the surface of the mesoporous PCH material [27]. By increasing the calcination temperature, the PCH-400 sample showed an increased meso-porosity, and the highest micropore volume (0.261 cm^3/g) compared to PCH-200. This was confirmed by the broadening of the adsorption part of the corresponding isotherms. The pore size distribution showed that the pores of PCH material (**Fig. 2**a) were small, and bimodal character, ranging from 2 to 12 nm. In conclusion, the impact of heat as an effective technique in the synthesis of mesoporous PCH in combination with heat treatment at up to 400°C, resulted in a prolonged adsorption-desorption isotherm, moderate porosity and micropore volume [23,24].

Fig. 2c shows the mineralogical and crystallographic information of PCH samples identified by the changes in the intensities and scattering angles of the X-rays. Two-dimensional crystal plane diffractions (hk) and various mineral impurities were confirmed in the XRD patterns using Jade 6 software. In terms of peak intensity and structural changes found in all PCH samples, the clay exhibits the structural characteristics of a host clay mineral [20,27]. The PCH samples showed the main peaks at $2\theta = 8.9$ (001, 003), 17.9 (002), 19.9 (100), 20.9, 20.7(100), 26.7 (101) 27.8 (103), which matched well with the conventional patterns for the clay minerals and their lattice planes (Quartz and Muscovite JCPDS No # 46-1045 and 07-0042) [28]. The composite structure was no longer observed as it was delaminated by oxidation and local overheating of the templates at high temperatures. Overall, most of the changes in mineralogical formation and D spacing (± 0.2Å) showed a correlation with the calcination temperature. In addition, the formation of a 'House-of-cards' structure might have decreased the intensity of d_{001} reflectance and increased the intensity of d_{101} reflectance at

206 800°C calcination temperature. As can be observed in the inset figure in XRD, d_{101} and d_{001}
207 reflections were shifted lower to a higher degree at 200 to 400°C and then shifted back again
208 to a lower degree with high intensity at 800°C. This can be attributed to recrystallization and
209 clogging of the porous structures due to the high calcination temperature [23,24].

210 The FTIR spectra of the PCH samples at different temperatures showed similar
211 trends to the XRD pattern. As the calcination temperature increased, the intensity of the peaks
212 decreased, as shown in **Fig. 2**d. The OH stretching region and the OH inner group were
213 observed between 3300 and 4000 cm^{-1}. As observed, the OH stretching range of PCH was
214 also affected by the calcination temperature [29]. The decrease in this region could be due to
215 partial dehydration of the PCH material. **Fig. 2**d shows the asymmetry and symmetry of CH_2
216 stretching at 2980 and 2979 cm^{-1} whose intensity decreases slightly with increasing
217 temperature, but whose wavelength range does not change. Two bands at 1737 and 1590 cm^{-1}
218 corresponded to the CH stretching and H-O-H bending vibration. The spectral peaks in the IR
219 range between 1000 and 500 cm^{-1} were related to the vibrations of the tetrahedral and
220 octahedral units of the phyllosilicates. The peaks at the wavelengths 1046 and 565 cm^{-1} were
221 generated by Si-O stretching and Si-OH stretching, confirming the formation of a three-
222 dimensional silica network of the material [30]. The functional group band at 699 cm^{-1} was
223 recognized as the bending vibration of Al-Al-OH deformation. The band detected at 950 cm^{-1}
224 was attributed to the bending vibration of the Al-OH-Al functional group (see inset figure).
225 Thus, as the calcination temperature increased, the intensities and peak areas of the OH, Si-O,
226 and Al-O functional groups changed. Moreover, as the calcination temperature increased, the
227 FTIR spectra showed several changes, most notably, a decline in the intensities of the bands
228 at 3666, 804, and 565 cm^{-1}, which indicates the dehydroxylation of PCH. In a previous study,
229 Fernandez et al. [31] reported that the coordination of Al and Si in the crystal lattice of the
230 calcined clay significantly shifts when the calcination temperature increased from 600°C
231 (nearly 90% dehydroxylation) to 800°C (98% dehydroxylation). A comparable phenomenon

was observed in our study (see **Fig. 2d**). In general, heat slowly eliminates the hydroxyl groups in clay material, disordering its structure and causing it to transform into a more stable, high-temperature phase through recrystallization.

The thermal stability of the PCH samples was investigated using thermogravimetric analysis (TGA), as shown in **Fig. 3**. TGA is commonly used to investigate the temperature thresholds at which clay minerals retain their stability. The process by which clay releases water from interlayers by heating is called dehydroxylation and can be detected by TGA. Two primary weight losses were observed in the TGA profile of PCH: (1) the first weight loss (8 to 9%), which was attributed to the elimination of physisorbed water (50-150°C), (2) the second weight loss of hydroxyl groups from PCH columns and the dehydroxylation of the -OH group in the clay layers [32]. In the second stage of thermal decomposition, the PCH mass continued to decrease in the temperature range from 150 to 710°C. This normally occurs when aluminosilicate minerals are heated during the dehydroxylation process. The TGA curves also show that the thermal stability of the PCH samples increased with increasing calcination temperature. In addition, PCH-200 and PCH-800 were found to lose 17% and 10% weight, respectively, and it was also found that the percentage weight loss was reduced by increasing the calcination temperature. In a previous study, Zhou et al. [33] investigated the effects of calcination temperature on excavated London waste clay. They calcined clay samples for two hours at temperatures between 300 and 1000°C and identified kaolinite, illite, and montmorillonite. Dehydroxylation of kaolinite occurred in the temperature range of 350 to 600°C, while dehydroxylation of montmorillonite and illite occurred in the temperature range of 600 to 950°C.

According to this study, the calcination temperature significantly influenced the structural and chemical properties of the PCH samples. By increasing the temperature during the calcination process, the hydroxyl groups were slowly removed, which led to a disintegration of the layered clay structure. The result was a progressive shift from a highly

ordered crystalline structure to a disordered amorphous state, as shown by the initially decreasing and then shifting while increasing intensity of the individual X-ray diffraction peaks (see Fig. 2c). In addition, calcination led to significant changes in the BET surface area and porosity of the PCH (see Table 1). More specifically, heating the samples to a moderate temperature (400°C) significantly increased their BET-specific surface area and pore volume. This may be due to the elimination of water between the layers and the formation of very small pores. However, at calcination temperatures above 400°C, the BET-specific surface area and porosity could decrease due to sintering and compaction processes [34]. Calcination caused changes in the chemical makeup of the clays, resulting in the gradual removal of hydroxyl groups and the creation of oxide phases. In short, temperature can induce chemical changes like dihydroxylation, mineral impurities and the formation of oxide phases in clay materials [11], as shown in Fig. 2c and d. On the other hand, these structural and chemical alterations of calcined clays have significant consequences for their prospective uses in catalysis, adsorption, and ceramic production [24,34–36].

Upscaling the synthesis of PCH materials for industrial applications faces several challenges in terms of cost efficiency, scalability, and reproducibility, which can be addressed by optimizing synthesis parameters, and implementing scale-up strategies and stringent quality control measures. By overcoming these challenges, PCH materials can be used effectively in real-world applications and contribute to advances in catalysis, adsorption, and other areas. On the other hand, clay-based products are widely used in many industries, such as petroleum (drilling mud or fluid), construction (bricks and tiles), ceramics (pots and tableware), and paper (fillers and coatings). They are also used in paints, cosmetics, polymers, baths, coatings, and pharmaceutical formulations.

Calcination of PCH at the correct temperature plays an important role as it influences the formation of important active phases, strength and durability of the clay material. Among all samples, PCH-400 had the largest BET surface area (667 m^2/g), the

average pore volume (0.69 cm^3/g), and crystallite size (56 nm). PCH-200 had the lowest BET surface area (227 m^2/g), average pore volume (0.38 cm^3/g), and the average crystallite size was 31 nm. FTIR and XRD studies revealed differences in the height and size of the peaks in the stretching of the silica network and the bending of alumina as the calcination temperature increased. A significant improvement of the PCH material properties is possible by adjusting various parameters during the synthesis process. The results showed that calcination at different temperatures had the greatest influence on the crystallinity, BET surface area and pore volume of the PCH, which could also affect the catalytic activity of this material. However, the combustion of the organic carbon chain could also release a large amount of heat and affect the interlayer structure of PCH. The incompletely burned template material could also carbonize at high temperatures, which can lead to clogging of the inner channel. Further investigations can be carried out by changing the ratio of surfactant and cross-linking agent and functionalizing with amines of different lengths. Knowledge of these synthesis effects is useful for tailoring specific PCH materials for particular applications, such as NO_x reduction, CO_2 capture, contaminant adsorption, and removal.

Acknowledgments

This work was supported by the Research and Development Program of Ghent University Global Campus (GUGC), Korea. TGA data were obtained with support from the National Research Foundation (NRF) of Korea (Grant No: 2022K1A3A1A78091315).

Table 1. Textural properties of the PCH samples.

Sample	S_{BET} (m^2/g)[a]	D_{pore} (nm)	V_{total} (cm^3/g)	S_{micro} (m^2/g)[b]	D_{micro} (nm)[c]	V_{micro} (cm^3/g)[c]	Crystallite size (nm)[d]
PCH-200	227	3.82	0.38	-	0.64	0.074	31
PCH-400	667	4.16	0.69	102	0.57	0.261	56
PCH-600	505	4.12	0.46	109	0.55	0.178	41
PCH-800	468	4.32	0.50	81	0.58	0.182	44

[a] S_{BET}: BET specific surface area, V_{Total}: total pore volume, D_{pore}: average pore size, S_{micro}: micropore surface area, D_{micro}: micropore diameter, V_{micro}: micropore volume; [b] Obtained via the t-plot method; [c] Obtained via the Horvath-Kawazoe (HK) method; [d] Average crystallite size was calculated using XRD data by the Scherrer equation [37].

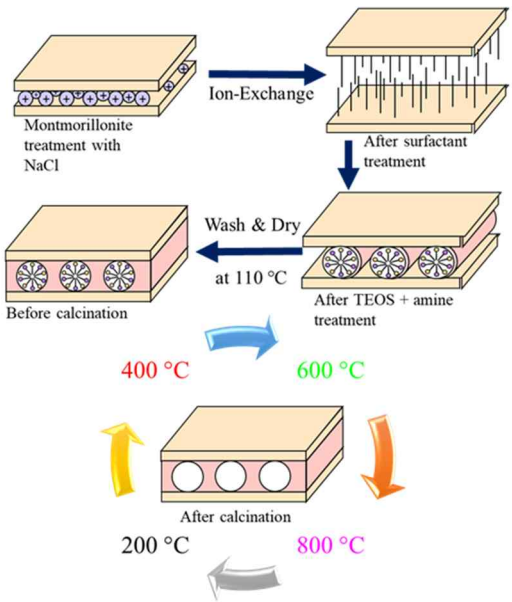

Scheme. 1 Schematic representation of PCH synthesis.

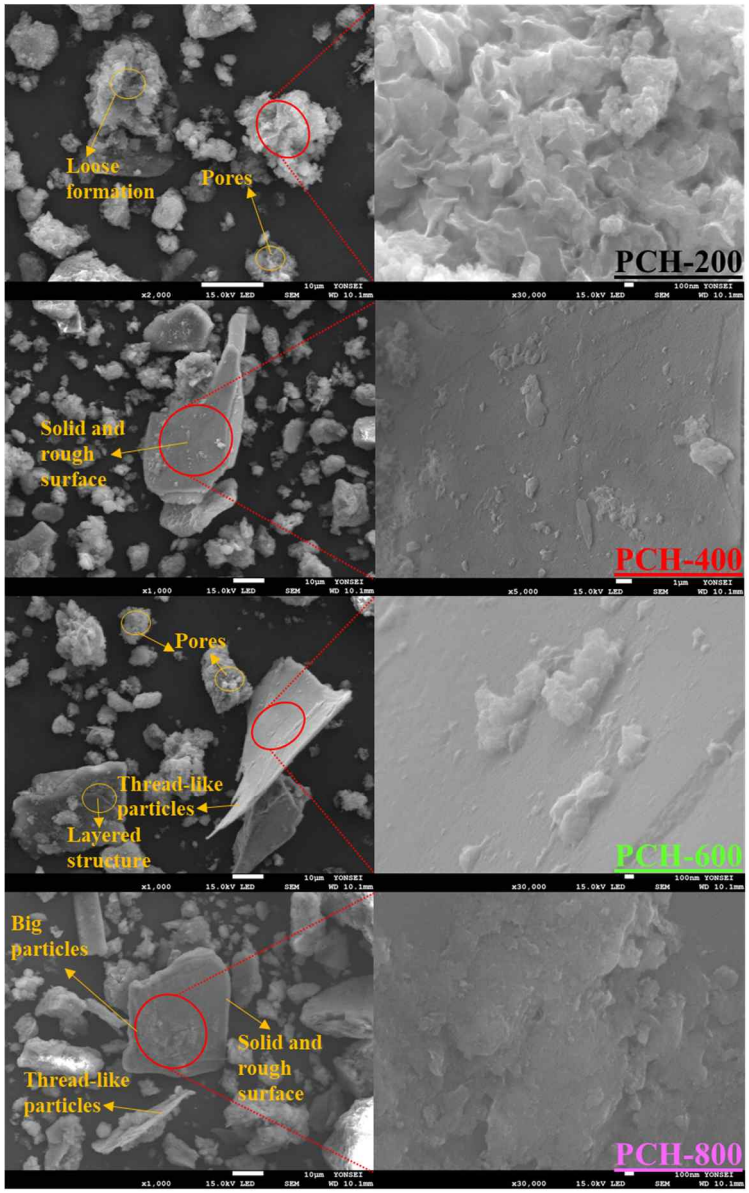

Fig. 1 SEM results for the synthesized PCH samples.

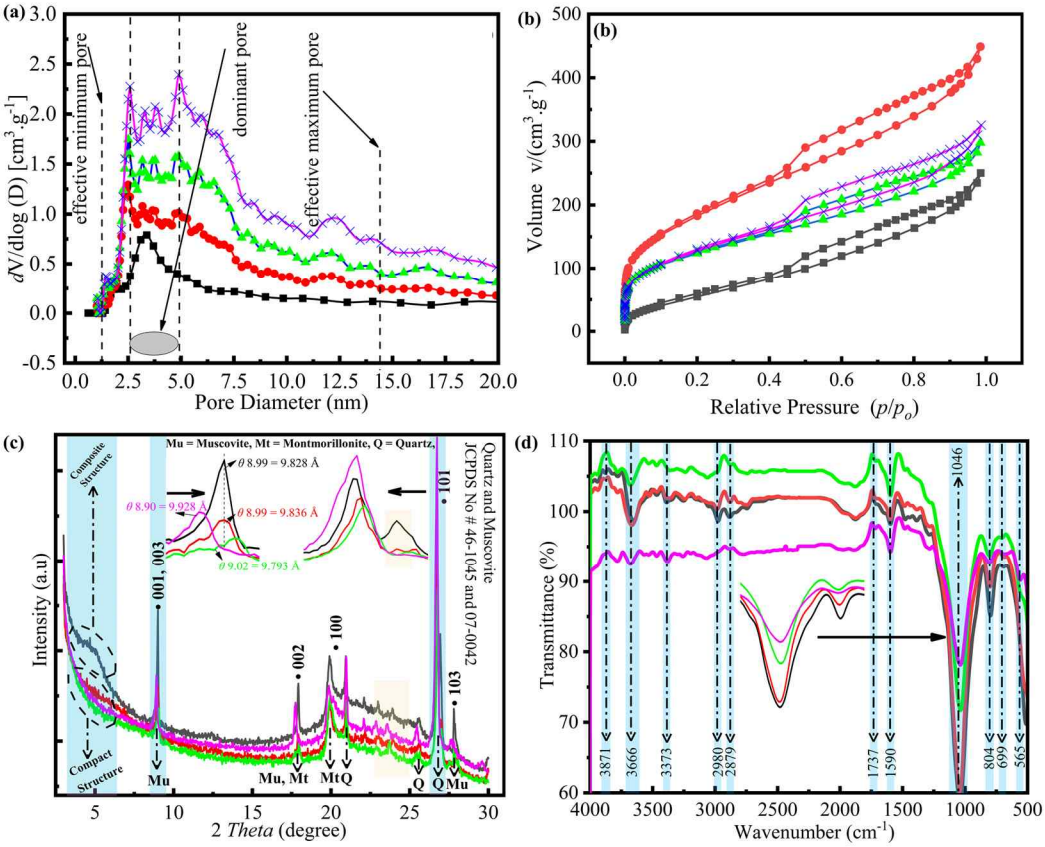

Fig. 2 PCH-200 (■), PCH-400 (■), PCH-600 (■), PCH-800 (■) samples (a) pore size distribution (b) N_2 adsorption-desorption isotherms (c) XRD patterns (d) FTIR analysis.

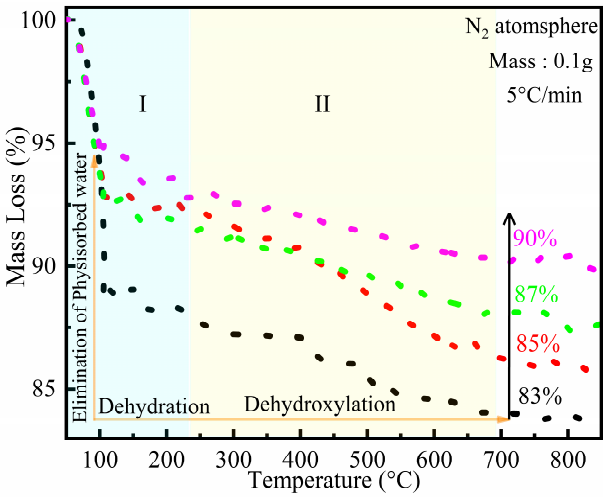

Fig. 3 Thermal analysis of PCH-200 (■), PCH-400 (■), PCH-600 (■), PCH-800 (■) samples.

References

[1] M. Kashif, M. Yuan, Y. Su, P.M. Heynderickx, A. Memon, A review on pillared clay-based catalysts for low-temperature selective catalytic reduction of NO_x with hydrocarbons, Appl Clay Sci 233 (2023). https://doi.org/10.1016/j.clay.2023.106847.

[2] M. Kashif, M.N. Khan, Y. Su, P.M. Heynderickx, Most efficient mesoporous Mn/Ga-PCH catalyst for low-temperature selective catalytic reduction of NO with C_3H_6, Vacuum 198 (2022). https://doi.org/10.1016/j.vacuum.2022.110879.

[3] E. Vilarrasa-García, J.A. Cecilia, D.C.S. Azevedo, C.L. Cavalcante, E. Rodríguez-Castellón, Evaluation of porous clay heterostructures modified with amine species as adsorbent for the CO_2 capture, Micropor Mesopor Mat 249 (2017). https://doi.org/10.1016/j.micromeso.2017.04.049.

[4] A. El Mouden, N. El Messaoudi, A. El Guerraf, A. Bouich, V. Mehmeti, A. Lacherai, A. Jada, J.H. Pinê Américo-Pinheiro, Removal of cadmium and lead ions from aqueous solutions by novel dolomite-quartz@Fe_3O_4 nanocomposite fabricated as nanoadsorbent, Environ Res 225 (2023). https://doi.org/10.1016/j.envres.2023.115606.

[5] Z. Ciğeroğlu, N. El Messaoudi, Z.M. Şenol, G. Başkan, J. Georgin, S. Gubernat, Clay-based nanomaterials and their adsorptive removal efficiency for dyes and antibiotics: A review, Mater Today Sustain 26 (2024). https://doi.org/10.1016/j.mtsust.2024.100735.

[6] A. El Mouden, N. El Messaoudi, A. El Guerraf, A. Bouich, V. Mehmeti, A. Lacherai, A. Jada, F. Sher, Multifunctional cobalt oxide nanocomposites for efficient removal of heavy metals from aqueous solutions, Chemosphere 317 (2023). https://doi.org/10.1016/j.chemosphere.2023.137922.

[7] N. El Messaoudi, D.S.P. Franco, S. Gubernat, J. Georgin, Z.M. Şenol, Z. Ciğeroğlu, D. Allouss, M. El Hajam, Advances and future perspectives of water defluoridation by adsorption technology: A review, Environ Res 252 (2024). https://doi.org/10.1016/j.envres.2024.118857.

[8] N. El Messaoudi, Z. Ciğeroğlu, Z.M. Şenol, A. Bouich, E.S. Kazan-Kaya, L. Noureen, J.H.P. Américo-Pinheiro, Green synthesis of nanoparticles for remediation organic pollutants in wastewater by adsorption, Adv Chem Pollut Environ Manag, 2024. https://doi.org/10.1016/bs.apmp.2023.06.016.

[9] N. El Messaoudi, Z. Ciğeroğlu, Z.M. Şenol, M. Elhajam, L. Noureen, A comparative review of the adsorption and photocatalytic degradation of tetracycline in aquatic environment by g-C_3N_4-based materials, J. Water Proc engineering 55 (2023). https://doi.org/10.1016/j.jwpe.2023.104150.

[10] T. Hanein, K.C. Thienel, F. Zunino, A.T.M. Marsh, M. Maier, B. Wang, M. Canut, M.C.G. Juenger, M. Ben Haha, F. Avet, A. Parashar, L.A. Al-Jaberi, R.S. Almenares-Reyes, A. Alujas-Diaz, K.L. Scrivener, S.A. Bernal, J.L. Provis, T. Sui, S. Bishnoi, F. Martirena-Hernández, Clay calcination technology: state-of-the-art review by the RILEM TC 282-CCL, Materials and Structures 55 (2022). https://doi.org/10.1617/s11527-021-01807-6.

[11] M.A. Harech, M. Mesnaoui, Y. Abouliatim, Y. Elhafiane, A. Benhammou, A. Abourriche, A. Smith, L. Nibou, Effect of temperature and clay addition on the thermal behavior of phosphate sludge, Boletin de La Sociedad Espanola de Ceramica y Vidrio 60 (2021). https://doi.org/10.1016/j.bsecv.2020.03.002.

[12] T.Y. Wibowo, A.Z. Abdullah, R. Zakaria, Effect of calcination temperature and Tmaoh on catalytic activity of basic clay, J Appl Sci 11 (2011). https://doi.org/10.3923/jas.2011.3619.3624.

[13] Y. Li, S. Yan, W. Yang, Z. Xie, Q. Chen, B. Yue, H. He, Effect of calcination temperature on structure and properties of Sn-Nb_2O_5/α-Al_2O_3 catalyst for ethylene oxide hydration, Catal Letters 124 (2008). https://doi.org/10.1007/s10562-008-9428-2.

[14] H. Al Dmour, F. Kooli, A. Mohmoud, Y. Liu, S.A. Popoola, Al and Zr porous clay heterostructures as removal agents of basic blue-41 dye from an artificially polluted solution: Regeneration properties and batch design, Materials 14 (2021). https://doi.org/10.3390/ma14102528.

[15] L. Chmielarz, A. Kowalczyk, M. Skoczek, M. Rutkowska, B. Gil, P. Natkański, M. Radko, M. Motak, R. Dębek, J. Ryczkowski, Porous clay heterostructures intercalated with multicomponent pillars as catalysts for dehydration of alcohols, Appl Clay Sci 160 (2018). https://doi.org/10.1016/j.clay.2017.12.015.

[16] F. Qu, L. Zhu, K. Yang, Adsorption behaviors of volatile organic compounds (VOCs) on porous clay heterostructures (PCH), J Hazard Mater 170 (2009). https://doi.org/10.1016/j.jhazmat.2009.05.027.

[17] J.E. Aguiar, J.A. Cecilia, P.A.S. Tavares, D.C.S. Azevedo, E.R. Castellón, S.M.P. Lucena, I.J. Silva, Adsorption study of reactive dyes onto porous clay heterostructures, Appl Clay Sci 135 (2017). https://doi.org/10.1016/j.clay.2016.09.001.

[18] R. Sanchis, J.A. Cecilia, M.D. Soriano, M.I. Vázquez, A. Dejoz, J.M. López Nieto, E. Rodríguez Castellón, B. Solsona, Porous clays heterostructures as supports of iron oxide for environmental catalysis, J Chem Eng 334 (2018). https://doi.org/10.1016/j.cej.2017.11.060.

[19] J.A. Cecilia, C. García-Sancho, F. Franco, Montmorillonite based porous clay heterostructures: Influence of Zr in the structure and acidic properties, Micropor Mesopor Mat 176 (2013). https://doi.org/10.1016/j.micromeso.2013.03.037.

[20] M. Kashif, M. Yuan, M. Abduallah, Y. Su, Fully selective catalytic oxidation of NO to NO_2 over most active Ga-PCH catalyst, J Environ Chem Eng 8 (2020). https://doi.org/10.1016/j.jece.2019.103524.

[21] M. Kashif, A. Halepoto, A. Memon, Y. Su, M. Abduallah, M.Y. Soomro, Gallium oxide impregnated on porous clay heterostructures material for selective catalytic reduction of nitrogen oxide with C_3H_6, J Environ Chem Eng 8 (2020). https://doi.org/10.1016/j.jece.2020.103943.

[22] R. El-Sheikhy, A. Al-Khuraif, M. Al-Shamrani, Converting polymer-wastes to green nanocomposites in Saudi Arabia: Investigation of fracture parameters (K_{Ic}, K_{IIc}, θ_c, σ_c) for quality and sustainability evaluation, Vacuum 217 (2023). https://doi.org/10.1016/j.vacuum.2023.112513.

[23] M. Benjelloun, P. Cool, P. Van Der Voort, E.F. Vansant, Template extraction from porous clay heterostructures: Influence on the porosity and the hydrothermal stability of the materials, Phys Chem Chem Phys 4 (2002) 2818–2823. https://doi.org/10.1039/b108361a.

[24] L. Chmielarz, B. Gil, P. Kuśtrowski, Z. Piwowarska, B. Dudek, M. Michalik, Montmorillonite-based porous clay heterostructures (PCHs) intercalated with silica-titania pillars-synthesis and characterization, J Solid State Chem 182 (2009) 1094–1104. https://doi.org/10.1016/j.jssc.2009.02.017.

[25] F. Kooli, Y. Liu, K. Hbaieb, R. Al-Faze, Preparation and catalytic activities of porous clay heterostructures from aluminium-intercalated clays: effect of Al content, Clay Miner 52 (2017). https://doi.org/10.1180/claymin.2017.052.4.09.

[26] M. Arai, S.L. Guo, M. Shirai, Y. Nishiyama, K. Torii, The catalytic activity of platinum-loaded porous smectite-like clay minerals containing different divalent cations for butane hydrogenolysis and ethylene hydrogenation, J Catal 161 (1996). https://doi.org/10.1006/jcat.1996.0232.

[27] J.A. Cecilia, C. García-Sancho, E. Vilarrasa-García, J. Jiménez-Jiménez, E. Rodriguez-Castellón, Synthesis, Characterization, Uses and Applications of Porous Clays Heterostructures: A Review, Chem Rec 18 (2018) 1085–1104. https://doi.org/10.1002/tcr.201700107.

[28] R. Sahu, M.K. Gupta, R. Chaturvedi, S.S. Tripaliya, A. Pappu, Moisture resistant stones waste based polymer composites with enhanced dielectric constant and flexural strength, Compos B Eng 182 (2020). https://doi.org/10.1016/j.compositesb.2019.107656.

[29] M. Kaur, S. Singh, R. Mehta, Physico-chemical modification induced in PLGA/OMMT nanocomposite films by Li^{3+} ion beam, Vacuum 125 (2016). https://doi.org/10.1016/j.vacuum.2015.12.018.

[30] F. Kooli, Y. Liu, K. Hbaieb, R. Al-Faze, Characterization and catalytic properties of porous clay heterostructures from zirconium intercalated clay and its pillared derivatives, Micropor Mesopor Mat 226 (2016) 482–492. https://doi.org/10.1016/j.micromeso.2016.02.025.

[31] R. Fernandez, F. Martirena, K.L. Scrivener, The origin of the pozzolanic activity of calcined clay minerals: A comparison between kaolinite, illite and montmorillonite, Cem Concr Res 41 (2011). https://doi.org/10.1016/j.cemconres.2010.09.013.

[32] J. Geng, Q. Sun, Effects of high temperature treatment on physical-thermal properties of clay, Thermochim Acta 666 (2018). https://doi.org/10.1016/j.tca.2018.06.018.

[33] D. Zhou, R. Wang, M. Tyrer, H. Wong, C. Cheeseman, Sustainable infrastructure development through use of calcined excavated waste clay as a supplementary cementitious material, J Clean Prod 168 (2017). https://doi.org/10.1016/j.jclepro.2017.09.098.

[34] S.N. Monteiro, C.M.F. Vieira, Influence of firing temperature on the ceramic properties of clays from Campos dos Goytacazes, Brazil, Appl Clay Sci 27 (2004). https://doi.org/10.1016/j.clay.2004.03.002.

[35] N. Saikumari, S.M. Dev, S.A. Dev, Effect of calcination temperature on the properties and applications of bio extract mediated titania nano particles, Sci Rep 11 (2021). https://doi.org/10.1038/s41598-021-80997-z.

[36] M. Abubakar, A. Muthuraja, N. Ahmad, Experimental investigation of the effect of temperature on the density of kaolin clay, Mater Today Proc, 41, 2020. https://doi.org/10.1016/j.matpr.2020.08.565.

[37] A. Monshi, M.R. Foroughi, M.R. Monshi, Modified Scherrer Equation to Estimate More Accurately Nano-Crystallite Size Using XRD, WJNSE 02 (2012). https://doi.org/10.4236/wjnse.2012.23020.